An intravascular immune response to *Borrelia burgdorferi* involves Kupffer cells and *i*NKT cells

Woo-Yong Lee[1], **Tara J Moriarty**[2], **Connie H Y Wong**[1], **Hong Zhou**[1], **Robert M Strieter**[4], **Nico van Rooijen**[5], **George Chaconas**[2,3], and **Paul Kubes**[1]

[1]Department of Physiology & Pharmacology, University of Calgary, Alberta, Canada [2]Department of Biochemistry & Molecular Biology, University of Calgary, Alberta, Canada [3]Department of Microbiology and Infectious Diseases, University of Calgary, Alberta, Canada [4]Department of Medicine, University of Virginia, Charlottesville, Virginia, USA [5]Department of Molecular Cell Biology, Free University, Amsterdam, The Netherlands

Abstract

Here we investigate the dynamics of the hepatic intravascular immune response to a pathogen relevant to invariant natural killer T cells (*i*NKT cells). Immobilized Kupffer cells with highly ramified extended processes into multiple sinusoids could effectively capture blood-borne, disseminating *Borrelia burgdorferi*, creating a highly efficient surveillance and filtering system. After ingesting *B. burgdorferi*, Kupffer cells induced chemokine receptor CXCR3–dependent clustering of *i*NKT cells. Kupffer cells and *i*NKT cells formed stable contacts via the antigen-presenting molecule CD1d, which led to *i*NKT cell activation. An absence of *i*NKT cells caused *B. burgdorferi* to leave the blood and enter the joints more effectively. *B. burgdorferi* that escaped Kupffer cells entered the liver parenchyma and survived despite Ito cell responses. Kupffer cell–*i*NKT cell interactions induced a key intravascular immune response that diminished the dissemination of *B. burgdorferi*.

The vasculature that perfuses all organs is made up of a considerable number of blood vessels necessary for tissue homeostasis, but this creates vulnerability to the dissemination of invading bacteria. This requires that the host immune system remain vigilant and pro-active, preventing pathogen dissemination. Although it is becoming clear that a diversity of cells of the immune response reside in the vasculature (called 'intravascular immunity' here), the mechanisms to prevent dissemination have not been fully elucidated, mainly

because of the imaging techniques needed to study this dynamic environment. Published studies have identified populations of patrolling cells of the immune response that probably function as sentries for the detection of bacteria in blood[1,2].

One such population is the natural killer T cells, which are a sub-population of T lymphocytes that express a T cell antigen receptor (TCR) with an invariant variable α-segment 14–joining α-segment 18 ($V_\alpha 14$-$J_\alpha 18$) TCRα chain paired with a restricted subset of TCR V_β chains in mice ($V_\alpha 24$-$J_\alpha 18$ or $V_\beta 11$ in humans) referred to as 'invariant natural killer T cells' (iNKT cells)[3]. The highly restricted repertoire of TCRs recognizes lipid antigens presented by CD1d[4,5], a nonclassical major histocompatibility complex class I–like antigen-presenting molecule. The first iNKT antigen identified was α-galactosylceramide (α-GalCer)[6] derived from *Agelas mauritianus*, a marine sponge, which so far remains the most potent antigen. Several lipid antigens from pathogens have since been reported, including one from *Borrelia burgdorferi*, a spirochete responsible for human Lyme disease[7,8].

The iNKT cells live mainly in a unique environment in the liver sinusoids but can also be found in the spleen and lungs and in small amounts in the lymph nodes. The liver sinusoids form an extensive network of narrow capillaries that serves as a filter to prevent the trafficking of pathogens via the blood for dissemination to other organs such as the joints[9]. Kupffer cells found in the liver vasculature capture and ingest pathogens and can present antigen *in vitro* via CD1d[10]. The sinusoidal endothelium is fenestrated, with large holes that antigens can easily permeate and attach to hepatocytes, dendritic cells and Ito (stellate) cells in the extravascular space for antigen presentation. Many groups have attempted to mimic this system *in vitro* and have shown that endothelium, Ito cells and dendritic cells express CD1d and can present antigen to iNKT cells, which leads to their activation and production of interferon-γ (IFN-γ) and/or interleukin 4 (IL-4). However, with multiple anatomical compartments in liver, it remains unclear which cells under what conditions capture pathogens and present antigens to iNKT cells *in vivo*.

Imaging of the intravascular immune response *in vivo* to α-GalCer, which would exclusively bind CD1d on all liver cells, has shown a cessation of iNKT cell crawling and more production of IL-4 and IFN-γ[1]. Unlike a specific CD1d ligand, an intact pathogen has many activating molecules, ranging from Toll-like receptor ligands to chemoattractants. In the liver, a pathogen will come in contact with or be captured by only a few appropriately positioned cells of the immune response in the vasculature (Kupffer cells, iNKT cells, neutrophils, monocytes and endothelium), whereas cells in the extravascular space of Dissé (for example, Ito cells) would be unlikely to interact with pathogens in blood. If pathogens escaped the bloodstream and entered the space of Dissé, then extravascular cells could potentially serve an important role in pathogen capture and antigen presentation. So far, systematic imaging assessment of iNKT cell responses to live pathogens in the vasculature and the contributions of partner cells of the immune response has not been done. Here we used multichannel- fluorescence spinning-disk microscopy with three-dimensional reconstruction capabilities *in vivo* to systematically examine the roles of Kupffer cells, Ito cells, endothelium and iNKT cells in the liver vasculature in response to live *B. burgdorferi*.

RESULTS

Activity of *i*NKT cells and Kupffer cells in sinusoids

We visualized the distribution of *i*NKT cells in the hepatic microvasculature of *Cxcr6*[gfp/+] mice, in which a gene encoding green fluorescent protein (GFP) is 'knocked into' one allele of the gene encoding the chemokine receptor CXCR6 and most GFP^{+} cells are *i*NKT cells[1]. We found that *i*NKT cells crawled in sinusoids in a random pattern, at times changing directions 180° (Fig. 1a,b and Supplementary Videos 1 and 2). Some investigators have suggested that one crawling population of leukocytes in the liver is Kupffer cells[11], but other investigators have subsequently reported that Kupffer cells are immobilized in the vasculature[12,13]. Our results showed that cells stained with a phycoerythrin-conjugated antibody to the surface antigen F4/80 (a pan-macrophage marker) were large, completely immobilized, ramified cells with extensions in as many as five sinusoids, giving a star-like appearance (Fig. 1c and Supplementary Video 3). Essentially all *i*NKT cells (Fig. 1a,b,d) and Kupffer cells (Fig. 1c–e) were in the hepatic sinusoids. Very few *i*NKT cells resided in venules, as *i*NKT cells that moved into post-sinusoidal venules were often swept away (Supplementary Video 4). The F4/80^{+} Kupffer cells captured dextran labeled with 2-megadalton tetramethylrhodamine (Fig. 1e), which is known to be sequestered by macrophages[14], thus demonstrating the selective rapid binding of foreign soluble molecules by Kupffer cells. Every sinusoid seemed to have at least one Kupffer cell or ramification immobilized in the lumen (Fig. 1c,e), which suggested a tremendous potential to filter the blood. Thus, whereas *i*NKT cells crawled, Kupffer cells were stationary, but both resided mainly in the sinusoids.

Foreign particle interactions in sinusoids

To explore whether the immobilized Kupffer cells were indeed responsible for the filtration of blood, we injected fluorescent inert beads or *Escherichia coli* directly into the bloodstream. Many inert beads (Figs. 1e and 2a–c) and *E. coli* (Fig. 2c) were captured rapidly (within seconds of injection) by Kupffer cells (Supplementary Video 5). Neither *i*NKT cells nor sinusoidal endothelial cells (SECs) interacted with the beads or *E. coli* (Fig. 2c). Next we injected *B. burgdorferi*, a microorganism known to activate *i*NKT cells via CD1d ligands. We found that *i*NKT cells did not bind *B. burgdorferi* (Fig. 2d), whereas Kupffer cells were again extremely effective at trapping this pathogen (15.6 ± 1.1 *B. burgdorferi* per field of view (FOV)). A very small but consistent number of spirochetes adhered to SECs (2.8 ± 0.6 *B. burgdorferi* per FOV; Fig. 2d,e). *B. burgdorferi* attached to Kupffer cells were completely immobilized, in contrast to those interacting with endothelium, which showed reciprocal translational motility over 10–20 μm (Supplementary Video 6). Those *B. burgdorferi* that bound to endothelium ultimately migrated out of the vasculature. We visualized one spirochete in the process of leaving the vessel with the tail still inside the sinusoid (Fig. 2f, arrowhead), whereas another spirochete had emigrated out of the vasculature (Fig. 2f, arrow).

We imaged intravascular immune responses to *B. burgdorferi* for the first 24 h after spirochete injection at intervals of 2–4 h. To measure how many spirochetes were captured and phagocytosed by Kupffer cells, we administered GFP-expressing *B. burgdorferi* to mice

whose Kupffer cells were labeled with phycoerythrin-conjugated antibody to F4/80 (anti-F4/80). The spirochetes seemed intact and green when first binding to Kupffer cells; however, by 2 or 5 h, they appeared as much smaller yellow particles (Fig. 3a), which indicated that they were either bound or ingested by the Kupffer cells. Bound and phagocytosed *B. burgdorferi* were indistinguishable by two-dimensional microscopy and we have presented these data as total interactions (Fig. 3b). By *z*-stack reconstruction (Fig. 3c) we determined that many of the spirochetes were inside Kupffer cells (enlarged, rotated view of Fig. 3c is presented in Supplementary Fig. 1) at 2 h and 5 h and diminished after that time point (Fig. 3d).

We also used *Cx3cr1*[gfp/+] mice (in which a gene encoding GFP is 'knocked into' one allele of the gene encoding the chemokine receptor CX3CR1) to visualize *B. burgdorferi* expressing the red fluorescent protein Tomato with GFP^{+} dendritic cells[15]. Unexpectedly, we detected two very distinct CD11c^{+} and CD11c^{−} populations of GFP^{+} cells in the liver (Fig. 3e–g). The CD11c^{−} population corresponded to very large stellate cells also known as Ito cells[16] (Fig. 3e–g). The dendritic cells were CD11c^{+} and were much smaller than the Ito cells and constituted only a small proportion of the GFP^{+} cells (Fig. 3e–g). Ito cells were present outside the blood vessels (Fig. 3h), and a *z*-stack reconstruction showed that the Ito cells had a spider-like appearance surrounding individual sinusoids (Fig. 3i), as reported before[16]. Very few Ito or dendritic cells were associated with Tomato-expressing *B. burgdorferi* (Fig. 3h, arrows) at 2 h or 5 h, with slightly more at 8 h and 12 h after spirochete injection (Fig. 3b). Notably, *z*-stack reconstruction of images of the Ito cells and spirochetes showed that fewer Ito cells than Kupffer cells ingested *B. burgdorferi* (Fig. 3c,i,j; quantification, Fig. 3d).

Antigen presentation to *i*NKT cells

To examine functional antigen presentation, we cultured liver-derived lymphocytes from uninfected mice for 5 or 8 h together with either Kupffer cells or Ito cells from mice infected with *B. burgdorferi*. Both Kupffer cells and Ito cells expressed abundant CD1d (Supplementary Fig. 2), and both cell types from *B. burgdorferi*–infected mice induced more IFN-γ production from lymphocytes (Fig. 4a). As a more specific marker of *i*NKT cell activation, we monitored CD69 upregulation. Kupffer cells and, to a much lesser extent, Ito cell, increased CD69 expression (Fig. 4b). When we cultured purified *i*NKT cells (>95%) together with either Kupffer cells or Ito cells, only Kupffer cells activated *i*NKT cells, as seen by CD69 upregulation (Fig. 4c). Longer culture for 12 h (data not shown), 24 h (Supplementary Fig. 3a) or 4 d (Fig. 4c) produced nearly identical results. Blocking CD1d completely inhibited *i*NKT cell activation by Kupffer cells (Fig. 4c). Measurement of IFN-γ secretion showed a similar trend, but because of the limited number of *i*NKT cells (50,000 cells per well), the amount of IFN-γ produced was very low. Nevertheless, the amount of IFN-γ produced by *i*NKT cells in the presence of Kupffer cells was lower in the presence of anti-CD1d (Supplementary Fig. 3b), but the amount produced by Ito cells was not (data not shown). Thus, Kupffer cells seem to be the predominant cells that present *B. burgdorferi*–derived antigens.

Activity of *i*NKT cells in response to *B. burgdorferi*

Published work has demonstrated that *i*NKT cells are activated and undergo crawling arrest in sinusoids by CD1d ligand–dependent and CD1d ligand–independent mechanisms[1,17]. Under basal conditions, CXCR6-GFP+ cells actively crawled within hepatic sinusoids with velocities that ranged from 0 μm/min to over 30 μm/min, with an average velocity of 15.8 ± 0.9 μm/min (Fig. 5a and Supplementary Videos 1 and 2). We noted much lower velocities for *i*NKT cells at 5 h, 8 h and 12 h (Supplementary Fig. 4a–c) and 24 h (Fig. 5b) after *B. burgdorferi* infection. In fact, 80% of *i*NKT cells were stationary, and the remaining 20% of *i*NKT cells crawled at a velocity of less than 5 μm/min at all times after infection. Clusters of *i*NKT cells formed stable contacts with Kupffer cells containing *B. burgdorferi* at 8 h (Fig. 5c) and 12 h (data not shown). Once firm adhesion occurred, the *i*NKT cells ceased to crawl and scan other Kupffer cells. The clusters grew in size (15–50 *i*NKT cells per cluster) over the 24-hour infection period (Fig. 5d and Supplementary Videos 7 and 8). A *z*-stack reconstruction of Kupffer cells and *i*NKT cells showed intimate contact between these cells (Fig. 5e), yet clustered *i*NKT cells seemed completely 'oblivious' to nearby spirochetes that were interacting with adjacent SECs (Fig. 5e, arrows). We also noted 'to and fro' motility of spirochetes on SECs that preceded emigration (Supplementary Videos 7 and 8). These results highlight the dependence of *i*NKT cells on antigen-presenting cells such as Kupffer cells for recognition of pathogens.

It is known that *i*NKT cells release large amounts of IFN-γ, IL-4 and other cytokines in response to CD1d ligands. The serum concentration of IFN-γ but not IL-4 was significantly higher as early as 5 h after spirochete injection (Fig. 5f). However, unlike results obtained with α-GalCer or other CD1d agonists, we also observed the early increase in IFN-γ in CD1d-deficient mice, which lack *i*NKT cells; this suggested that other cells responded to the infection at this early stage. Serum IFN-γ reached a peak concentration of 177.3 ± 24.8 pg/ml at 8 h (this is about eight times the concentration under basal conditions), and this higher IFN-γ expression was completely eliminated in CD1d-deficient mice (*Cd1d1*−/−; called '*Cd1d*−/−' here (Fig. 5f). IFN-γ concentrations decreased by 24 h after infection in both wild-type and *Cd1d*−/− mice, but *Cd1d*−/− mice continued to express less IFN-γ (Fig. 5f). Hepatic IFN-γ concentrations paralleled those in the plasma in wild-type mice. We found no increase in IFN-γ concentrations in *i*NKT-deficient livers (Supplementary Fig. 5). Thus, *i*NKT cells adhered to *B. burgdorferi*–containing Kupffer cells and began to produce IFN-γ.

We next investigated the role of chemokines and CD1d in the cluster formation, crawling velocity and stationary arrest. *B. burgdorferi*– infected mice that received pertussis toxin (PTX) had complete inhibition of clustering (Fig. 6a,b) and a much greater crawling velocity profile (Supplementary Fig. 6a,b). The average crawling velocity was fivefold greater for infected mice treated with PTX than for infected mice that did not receive PTX (Fig. 6c), and the number of arrested cells was significantly lower (Fig. 6d). These data suggest that the clustering was achieved through a G protein–coupled receptor, probably because of chemokines. CXCR3 and CXCR6 are two chemokine receptors expressed on *i*NKT cells that induce a strong chemotactic response *in vitro*[18]. Published work has reported that CXCR6 deficiency does not affect *i*NKT cell crawling activity but enhances cell survival[1].

Blocking CXCR3, however, inhibited the formation of iNKT cell clusters by *B. burgdorferi* in the liver by more than 90% (Fig. 6b) and resulted in a greater crawling velocity profile (Supplementary Fig. 6c,d) and average crawling velocity (Fig. 6c) and a lower number of arrested cells (Fig. 6d) relative to those of infected mice that did not receive anti-CXCR3. Kupffer cells infected with *B. burgdorferi* and isolated 8 h later released substantial amounts of the CXCR3 receptor ligand CXCL9 (MIG), whereas noninfectious bacterial strains grown in the absence of blood produced no CXCL9 and failed to induce clusters (data not shown).

Treatment with anti-CD1d likewise resulted in less iNKT cell clustering and greater iNKT cell velocity in the *B. burgdorferi*–infected mice (Fig. 6 and Supplementary Fig. 6c). We found small clusters of iNKT cells in the anti-CD1d-treated mice, but the cells were not arrested and continued to crawl in a small area, probing Kupffer cells (Supplementary Video 9). Treatment with α-GalCer induced iNKT cell arrest (Fig. 6c,d) but failed to cause iNKT cell clustering (Fig. 6b), which highlights the complexity of the response to a whole pathogen versus a single CD1d ligand.

We counted liver iNKT cells by flow cytometry as well as iNKT cells per FOV and found only a subtle increase in the total number of iNKT cells over the first 24 h after infection (Fig. 6e), consistent with the idea that iNKT proliferation occurs after 48–72 h of exposure to CD1d ligands[19]. Moreover, PTX, anti-CXCR3 or anti-CD1d did not affect the number of iNKT cells in the liver (Fig. 6f). Thus, inhibition of clustering was not due to depletion of iNKT cells by any of the aforementioned inhibitors.

B. burgdorferi and the role of macrophages and *i*NKT cells

To assess the role of Kupffer cells and iNKT cells, we used clodronate liposomes (CLLs) and $Cd1d^{-/-}$ mice, respectively. Kupffer cells are rapidly depleted by intravenous injection of CLLs[20]. We noted profound depletion of Kupffer cells in the hepatic sinusoids at 24–72 h after treatment with 200 μl CLLs (0.69 mol/l, as clodronate; Fig. 7a). Most spirochetes were removed from vehicle-treated liver at 12 h and 24 h after injection of GFP-expressing *B. burgdorferi*, whereas large numbers of *B. burgdorferi* interacting in liver sinusoids remained in CLL-treated mice (Fig. 7b and Supplementary Video 10). Most spirochetes were freely translocating and did not show the pattern of immobilization observed after adhesion to Kupffer cells in untreated mice. As a result, we observed very large numbers of *B. burgdorferi* in the blood (Fig. 7c) and in the liver parenchyma by 3 d in CLL-treated mice (Table 1). In the absence of Kupffer cells, iNKT cells had a higher crawling velocity (Fig. 7d) and failed to produce clusters (Fig. 7e). Less than 50% of iNKT cells were stationary at 5 h (Fig. 7d), but 80% arrested at 24 h after infection (data not shown), which suggested that other cells are able to release endogenous activating mediators or present *B. burgdorferi* glycolipids. The early iNKT cell–independent increase in IFN-γ was still evident in Kupffer cell–depleted mice after *B. burgdorferi* injection, but the iNKT cell–dependent production of IFN-γ was completely inhibited (Supplementary Fig. 5), which further supports the idea of a need for Kupffer cell–iNKT cell interactions. A small percentage of mice depleted of Kupffer cells succumbed to *B. burgdorferi* infection by 24 h, but no mice died after that time point. All wild-type mice survived (Fig. 7f). CLLs have been used to deplete the spleen of macrophages[21] in addition to Kupffer cells, so the results seen after CLL treatment could

have been due to loss of all phagocytic cells. Splenectomy, however, did not explain all the effects we saw in CLL-treated mice (Fig. 7c and Table 1).

The removal of Kupffer cells with CLLs resulted in greatly enhanced binding of *B. burgdorferi* to endothelium, and many spirochetes were located in liver parenchyma at 24 h (Fig. 7g) and 3 d (Table 1). The spleen also trapped spirochetes via macrophages (Supplementary Fig. 7) but had a much smaller load of spirochetes at 3 d than did the liver, which had the largest load of spirochetes (Supplementary Table 1) even after normalization for tissue weight (Table 1). Removal of the spleen did not increase bacteremia (Fig. 7c), which suggested that the liver was able to clear *B. burgdorferi* from blood even in the absence of the spleen (Table 1).

Finally, we examined the importance of *i*NKT cells in *B. burgdorferi* infection. In the absence of *i*NKT cells, we noted much more accumulation of *B. burgdorferi* in the joints (Table 1), a bacterial burden 26-fold above that of wild-type mice and four- to fivefold above that of mice treated with CLLs. The spirochetes were also more abundant in the bladder and liver but not in other organs (spleen) and were actually lower in abundance in the heart (Table 1). This result may reflect initial tropism for organs such as the joints and liver. In addition, we found some *B. burgdorferi* in the blood of wild-type mice, whereas in the absence of *i*NKT cells, we found almost no spirochetes in the blood (Fig. 7c) and we found many more in various tissues in *Cd1d*^{−/−} mice (Table 1), which suggested that *i*NKT cells limit the emigration of *B. burgdorferi* out of the vasculature. Notably, Kupffer cell capture (Supplementary Fig. 8a), phagocytosis (Supplementary Fig. 8b) or killing (data not shown) of *B. burgdorferi* over the first few hours after infection was not affected by the loss of *i*NKT cells. This result rules out the possibility of an indirect effect of *i*NKT cells on Kupffer cells as a reason for the greater load of *B. burgdorferi* in *Cd1d*^{−/−} mice.

DISCUSSION

By multichannel-fluorescence spinning-disk microscopy, we visualized Kupffer cells here as an immobilized population of ramified macrophages that extended processes into as many as five sinusoids, thus demonstrating extensive filtering capacity of each of these vessels. These cells had an exquisite capacity for capturing foreign substances, including soluble molecules, inert beads and bacteria[12]. Notably, we did see a very small intravascular crawling monocyte population in the liver of *Cx3cr1*[gfp/+] mice such as that described in the skin, mesentery and brain[2,22], which suggests that Kupffer cells may replace those cells in the liver. After infection, the activity of *i*NKT cells was substantially altered; *i*NKT cells slowed their crawling activity and arrested in clusters on Kupffer cells, which led to IFN-γ production. This clustering activity was prevented by the blockade of G protein–coupled receptors, by inhibition of CXCR3 or CD1d or by depletion of Kupffer cells. In the absence of Kupffer cells or *i*NKT cells, dissemination of *B. burgdorferi* occurred.

This report is an imaging-based systematic examination of *i*NKT activity in liver in response to an intact pathogen with known CD1d ligands. The differences in *i*NKT cell responses to pathogen versus CD1d ligand alone were striking. Although α-GalCer induced the production of IFN-γ and IL-4 by *i*NKT cells, *B. burgdorferi* induced only IFN-γ. Even at

day 7, only very small increases in IL-4 (from 1% to 2%) in response to *B. burgdorferi* have been reported[9]. It has been shown that α-GalCer causes rapid stopping of *i*NKT cells[1] but not the swarming activity that leads to *i*NKT clusters. Unlike α-GalCer, intact *B. burgdorferi* has multiple pathogen-associated molecular patterns that can activate pattern-recognition pathways, including Toll-like receptor 2 (ref. 23), in macrophages, which results in the release of chemokines that recruit effector leukocytes. Indeed, Kupffer cells produced CXCR3 ligands, including CXCL9, in response to *B. burgdorferi*, and Kupffer cell depletion prevented the formation of *i*NKT clusters. That finding is consistent with the fact that CXCR3 ligands are potent chemokines for *i*NKT cells *in vitro*[19]. The inhibition of G protein–coupled receptors (specifically CXCR3) also prevented clustering, which makes it tempting to suggest chemotaxis or directed migration. However, the possibility of the retention of *i*NKT cells randomly arriving at the site where chemokines are released from the Kupffer cells cannot be discounted. Unlike the thousands of neutrophils that swarm to sites of infection within 1–2 h, only 15–50 *i*NKT cells formed a cluster over 24 h, which allows either chemotaxis and/or chemokine retention of *i*NKT cells to be a potential role for CXCR3 ligands in this system. Nevertheless, there is an important role for CXCR3 ligands such as CXCL9 in *i*NKT cell clustering under flow conditions in the blood vessels in response to pathogens.

In this study we have demonstrated a role for Kupffer cells in the clearance of blood-borne *B. burgdorferi* from the vasculature. Indeed, macrophage and their subsets in liver (Kupffer cells) are professional phagocytes, recognizing pathogens and engulfing them into phagosomes, which mature into phagolysosomes[24,25]. Kupffer cells can then present glycolipid antigens via CD1d, as shown here. Although macrophages have extremely high microbicidal activity, other cells, including the endothelium, have a more limited capacity to phagocytose and digest *B. burgdorferi*. We observed no internalization of *B. burgdorferi* by SECs. We did see the adherence of a small proportion of spirochetes to SECs, and this was greatly exaggerated after depletion of Kupffer cells and when SECs were exposed to the pathogens. A lack of Kupffer cells led to further increases in *B. burgdorferi* in liver parenchyma, which is also consistent with the idea that these spirochetes use SECs as a portal to bypass the first line of defense (that is, the Kupffer cells) and successfully gain access to the extravascular space. These data also suggest that the Kupffer cells were not a portal for the entry of spirochetes into liver parenchyma, as shown before for other spirochetes, including *Plasmodium yoelii*[13].

Published reports have suggested that Ito cells could present antigen to *i*NKT cells *in vitro* and when CD1d-deficient mice are reconstituted with CD1d-sufficient Ito cells in the blood[26]. We did visualize some *B. burgdorferi* in close proximity to Ito cells, and in a few rare cases we saw Ito cells that had ingested spirochetes, but this was at times when *i*NKT cells were already activated. When we isolated Ito cells from *B. burgdorferi*–infected mice and cultured them together *in vitro* with lymphocytes, we detected some IFN-γ production, but this cytokine secretion was not dependent on *i*NKT cells or CD1d. We therefore propose that Ito cells located outside the vasculature act as a secondary line of defense against spirochetes that avoided ingestion by Kupffer cells. However, this system was not sufficient to eradicate *B. burgdorferi*. The spirochetes became particularly abundant in the liver, which suggested a failure to recognize and/or eradicate the pathogen, allowing a potential reservoir

in mice. Although such a reservoir has not been identified in humans, up to 60% of patients with Lyme disease present with a mild form of hepatitis[27,28]. From the accumulated data that large clusters of *i*NKT cells become activated after making intimate contact with Kupffer cells that have ingested *B. burgdorferi*, we conclude that Kupffer cells are the main antigen- presenting cells for *i*NKT cells in the liver vasculature for this particular pathogen. Although published studies have hinted at the possibility of intravascular antigen presentation, this is the first documented example, to our knowledge, of such an immune response in blood vessels.

Notably, although Ito cells did not seem to present antigen to *i*NKT cells during *B. burgdorferi* infection, Ito cells could in other infections use the holes in fenestrated endothelium as portals to reach out and activate *i*NKT cells, or *i*NKT cells could extend microvilli into the space of Dissé to contact Ito cells, a mechanism proposed for CD8$^+$ T cells and hepatocytes[29]. Moreover, the Ito cells would not need to be phagocytic. It is possible that Kupffer cells ingest *B. burgdorferi* and release glycolipids that could bind CD1d on Ito cells. It is also possible that the Kupffer cells and other cells induced the release of endogenous glycolipids that could be bound by Ito cells and presented to lymphocytes, as described for *Salmonella typhimurium*, which activates *i*NKT cells by inducing production of the endogenous lysosomal glycosphingolipid iGb3 (ref. 7). A role for these endogenous glycolipids could contribute to the immune response in *B. burgdorferi* infection.

The most obvious phenotype of *i*NKT cell–deficient mice was a much greater abundance of *B. burgdorferi* in the joints than that of mice treated with CLLs, which instead induced huge bacteremia. This finding highlights the different but important roles for Kupffer cells and *i*NKT cells. Kupffer cells function as phagocytes to remove *B. burgdorferi* from blood, whereas *i*NKT cells do not phagocytose *B. burgdorferi* but prevent the dissemination of pathogens to organs such as the joints. An absence of *i*NKT cells resulted in lower serum IFN-γ concentrations and greater movement of spirochetes out of the blood and into the tissues. *B. burgdorferi* numbers were even lower in the blood of *i*NKT cell–deficient mice than that of wild-type mice, perhaps reflecting the ease with which the spirochetes entered the tissues in *i*NKT cell–deficient mice. This result is consistent with our hypothesis that *i*NKT cells located in liver and spleen are sentinel cells in blood, detecting bacteremia and releasing factors that can induce long-distance effects in other tissues. Hematogenous dissemination is a critical step in the progression of all spirochete diseases[30], and it is likely that disseminating *B. burgdorferi* and other pathogens that express CD1d ligands have evolved mechanisms to evade intravascular immune surveillance in major blood filtration sites such as the liver. Our studies have also identified a subpopulation of *B. burgdorferi* that escaped the vast network of sinusoidal coverage provided by Kupffer cells via endothelial adhesion and extravasation. This observation suggests that vascular adhesion and emigration could constitute one of the strategies used by *B. burgdorferi* and other spirochetes to evade the potent intravascular innate immune response, resulting in the establishment of bacterial reservoirs in places such as the liver.

ONLINE METHODS

Mice

BALB/cJ and CD1d-deficient mice were from The Jackson Laboratory. *Cxcr6*[gfp/+] and *Cx3cr1*[gfp/+] knock-in mice on the BALB/cJ and C57BL/6 background, respectively, were gifts from D.R. Littman. All mice were maintained in a specific pathogen–free, double-barrier unit at the University of Calgary. Protocols were in accordance with guidelines drafted by the University of Calgary Animal Care Committee and the Canadian Council on the Use of Laboratory Animals. Mice used were between 8 and 12 weeks of age.

Intravital microscopy of the liver

Spinning-disk multichannel-fluorescence intravital microscopy of mouse liver was done as described[31,32]. *Cxcr6*[gfp/+] and *Cx3cr1*[gfp/+] mice[1,15] were used for the visualization of hepatic *i*NKT cells and Ito cells (dendritic cells) in the liver, respectively. Phycoerythrin-conjugated anti-F4/80 (1 μg per mouse; BM8; eBioscience) was injected intravenously into wild-type and *Cxcr6*[gfp/+] mice for imaging of Kupffer cells. Anti-PECAM-1 (3 μg per mouse; 390; eBioscience) was used for delineation of the liver vasculature. The activity of multiple cell types and bacteria in the hepatic microvasculature was assessed simultaneously with three laser excitation wavelengths in rapid succession (488 nm, 561 nm and 635 nm; Cobalt) and was visualized with the appropriate long-pass filters (Semrock). Typical exposure time for excitation wavelengths was 1.0 s. A back-thinned electron-multiplying charge-coupled device camera (512 × 512 pixels; C9100-13; Hamamatsu) was used for fluorescence detection. Volocity software (Improvision) was used for acquisition and analysis of images.

Bacterial strains

Fluorescent *E. coli* was provided by E. Allen-Vercoe. The GFP (pTM61) and Tomato (pTM201) expression plasmids were constructed as described[32] (Supplementary Methods). All *B. burgdorferi* strains were grown for 48 h in BSK-II medium prepared in-house[33] in the presence of 1% (vol/vol) mouse blood, except where noted otherwise[32]. For the generation of *B. burgdorferi* strain GCB776 (infectious Tomato), electrocompetent infectious *B. burgdorferi* was prepared from strain B31 5A4 NP1 (ref. 34) as described[32]. The construction of *B. burgdorferi* strains GCB726 (infectious GFP) and GCB705 (noninfectious GFP) has been reported[32]. In preliminary experiments, the immune responses of noninfectious GFP-expressing *B. burgdorferi* (strain GCB705) and *B. burgdorferi* grown in the absence of blood were assessed. Although the spirochetes and *i*NKT cells had very different morphology, to avoid possible confusion between GFP-expressing *B. burgdorferi* and GFP-expressing *i*NKT cells, in some cases the bacteria were labeled with Syto 60 and an indodicarbocyanine laser and 635-nm filter were used. In addition, success with Tomato expression in *B. burgdorferi* allowed confirmation of observations with a second label.

B. burgdorferi infection and treatment of mice

Mice were infected intravenously via the tail or jugular vein with various numbers of *B. burgdorferi* per mouse, and a dose of 1.0×10^8 *B. burgdorferi* was selected, as this permitted

observation of the interaction of substantial numbers of *B. burgdorferi* in sinusoids. Mice were able to clear this dose of bacteria within 24 h without any mortality. For investigation of the role of Kupffer cells in the activation of *i*NKT cells by *B. burgdorferi* infection, mouse livers were depleted Kupffer cells through the use of CLLs[20]. Clodronate (a gift from Roche Diagnostics) was incorporated (by N.v.R.) into liposomes (0.69 mol/l as clodronate)[20]. The intravenous administration of 200 μl 24 h before spirochete challenge was sufficient to remove Kupffer cells for at least 48 h, but 50 or 100 μl was not sufficient. Videos of the CLL-treated group were compared with those of the vehicle-treated group to assess the activity pattern of *i*NKT cells. For blockade of chemokine signaling, mice were injected intraperitoneally with 500 ng PTX at 1 d and 3 d before infection[35]. For selective blockade of CXCR3 or CD1d, 1 ml anti-CXCR3 was injected intraperitoneally or 50 μg anti-CD1d (1B1; eBioscience) was injected intravenously, respectively, 30 min before *B. burgdorferi* injection[36,37]. Anti-CXCR3 serum was prepared as described[37]. For analysis of whether α-GalCer mimics the formation of *i*NKT cell clusters by *B. burgdorferi*, 2 μg α-GalCer (Alexis Biochemicals) was injected intravenously 24 h before intravital microscopic observation[1,38].

For analysis of the ability to capture particulate *in vivo*, polychromatic microspheres (0.5×10^8 Polysciences), Syto 60–labeled or GFP-expressing *E. coli* (1.6×10^8), or Syto 60–labeled, GFP- or Tomato-expressing *B. burgdorferi* (1×10^8) were administered intravenously. These amounts allowed easy detection of interactions of host cells of the immune response and pathogens that happened within seconds of injection. The binding capacities of hepatic *i*NKT, Kupffer and endothelial cells were evaluated by intravital video imaging over a 1-hour period at 2 h, 5 h, 8 h, 12 h and 24 h after spirochete injection. The ingestion of GFP- or Tomato-expressing *B. burgdorferi* by phycoerythrin- labeled Kupffer cells, GFP^{+} Ito cells and dendritic cells was quantified by *z*-stack reconstruction.

Cytokine concentrations in serum and liver samples were measured by OptEIA enzyme-linked immunosorbent assay sets according to the manufacturer's instructions (BD Pharmingen).

Measurement of *B. burgdorferi* DNA in the tissue

Mice were killed 3 d after infection with *B. burgdorferi*, and organs and tissues were collected, weighed, snap-frozen in liquid nitrogen and stored at −80 °C. DNA was collected from preweighed tissue samples with a DNeasy kit according to the manufacturer's instructions (Qiagen).

DNA standards were prepared by amplification of a target *B. burgdorferi* DNA sequence (from the *flaB* gene) with quantitative PCR primers (Supplementary Methods) and cloning of the resulting PCR product into the pJET1.2/blunt cloning vector with the CloneJet PCR cloning kit (Fermentas).

A Bio-Rad IQ5 multicolor real-time PCR detection system was used for quantitative PCR with 2.5 μl pooled sample DNA in 25-μl reaction volumes according to methods and primers adapted from published studies in which quantitative PCR was used to quantify *Borrelia* in various host tissues[9,39].

Statistical analysis

Data were analyzed by standard statistical analysis (analysis of variance and Student's *t*-test with Bonferroni's correction for multiple comparisons where appropriate). Statistical significance was set at a *P* value of less than 0.05.

Additional methods

Information on spinning-disk confocal intravital microscopy, analysis of intravital imaging videos, *B. burgdorferi* transformation and screening, preparation of fluorescent *B. burgdorferi* for injection, quantitative analysis of phagocytic capacity, preparation and analysis of Kupffer cells, Ito cells and lymphocytes, and flow cytometry is available in the Supplementary Methods.

Supplementary Material

Refer to Web version on PubMed Central for supplementary material.

Acknowledgments

References

1. Geissmann F, et al. Intravascular immune surveillance by CXCR6^{+} NKT cells patrolling liver sinusoids. PLoS Biol. 2005; 3:e113. [PubMed: 15799695]

2. Auffray C, et al. Monitoring of blood vessels and tissues by a population of monocytes with patrolling behavior. Science. 2007; 317:666–670. [PubMed: 17673663]

3. Kronenberg M. Toward an understanding of NKT cell biology: progress and paradoxes. Annu Rev Immunol. 2005; 23:877–900. [PubMed: 15771592]

4. Kawano T, et al. CD1d-restricted and TCR-mediated activation of Vα14 NKT cells by glycosylceramides. Science. 1997; 278:1626–1629. [PubMed: 9374463]

5. Brossay L, et al. CD1d-mediated recognition of an α-galactosylceramide by natural killer T cells is highly conserved through mammalian evolution. J Exp Med. 1998; 188:1521–1528. [PubMed: 9782129]

6. Kobayashi E, Motoki K, Uchida T, Fukushima H, Koezuka Y. KRN7000, a novel immunomodulator, and its antitumor activities. Oncol Res. 1995; 7:529–534. [PubMed: 8866665]

7. Mattner J, et al. Exogenous and endogenous glycolipid antigens activate NKT cells during microbial infections. Nature. 2005; 434:525–529. [PubMed: 15791258]

8. Kinjo Y, et al. Natural killer T cells recognize diacylglycerol antigens from pathogenic bacteria. Nat Immunol. 2006; 7:978–986. [PubMed: 16921381]

9. Tupin E, et al. NKT cells prevent chronic joint inflammation after infection with *Borrelia burgdorferi*. Proc Natl Acad Sci USA. 2008; 105:19863–19868. [PubMed: 19060201]

10. You Q, Cheng L, Kedl RM, Ju C. Mechanism of T cell tolerance induction by murine hepatic Kupffer cells. Hepatology. 2008; 48:978–990. [PubMed: 18712788]

11. MacPhee PJ, Schmidt EE, Groom AC. Evidence for Kupffer cell migration along liver sinusoids, from high-resolution *in vivo* microscopy. Am J Physiol. 1992; 263:G17–G23. [PubMed: 1636711]

12. Egen JG, et al. Macrophage and T cell dynamics during the development and disintegration of mycobacterial granulomas. Immunity. 2008; 28:271–284. [PubMed: 18261937]

13. Baer K, et al. Kupffer cells are obligatory for *Plasmodium yoelii* sporozoite infection of the liver. Cell Microbiol. 2007; 9:397–412. [PubMed: 16953803]

14. Dory D, et al. Generation and functional characterization of a clonal murine periportal Kupffer cell line from H-2Kb-tsA58 mice. J Leukoc Biol. 2003; 74:49–59. [PubMed: 12832442]

15. Niess JH, et al. CX3CR1-mediated dendritic cell access to the intestinal lumen and bacterial clearance. Science. 2005; 307:254–258. [PubMed: 15653504]

16. Wake K. Hepatic stellate cells: Three-dimensional structure, localization, heterogeneity and development. Proc Jpn Acad Ser B. 2006; 82:155–164. [PubMed: 25792778]

17. Velázquez P, et al. Cutting edge: activation by innate cytokines or microbial antigens can cause arrest of natural killer T cell patrolling of liver sinusoids. J Immunol. 2008; 180:2024–2028. [PubMed: 18250405]

18. Johnston B, Kim CH, Soler D, Emoto M, Butcher EC. Differential chemokine responses and homing patterns of murine TCR αβ NKT cell subsets. J Immunol. 2003; 171:2960–2969. [PubMed: 12960320]

19. Wilson MT, et al. The response of natural killer T cells to glycolipid antigens is characterized by surface receptor down-modulation and expansion. Proc Natl Acad Sci USA. 2003; 100:10913–10918. [PubMed: 12960397]

20. van Rooijen N, Sanders A. Liposome mediated depletion of macrophages: mechanism of action, preparation of liposomes and applications. J Immunol Methods. 1994; 174:83–93. [PubMed: 8083541]

21. Junt T, et al. Subcapsular sinus macrophages in lymph nodes clear lymph-borne viruses and present them to antiviral B cells. Nature. 2007; 450:110–114. [PubMed: 17934446]

22. Audoy-Rémus J, et al. Rod-Shaped monocytes patrol the brain vasculature and give rise to perivascular macrophages under the influence of proinflammatory cytokines and angiopoietin-2. J Neurosci. 2008; 28:10187–10199. [PubMed: 18842879]

23. Bernardino AL, Myers TA, Alvarez X, Hasegawa A, Philipp MT. Toll-like receptors: insights into their possible role in the pathogenesis of Lyme neuroborreliosis. Infect Immun. 2008; 76:385–395.

24. Vieira OV, Botelho RJ, Grinstein S. Phagosome maturation: aging gracefully. Biochem J. 2002; 366:689–704. [PubMed: 12061891]

25. Savina A, Amigorena S. Phagocytosis and antigen presentation in dendritic cells. Immunol Rev. 2007; 219:143–156. [PubMed: 17850487]

26. Winau F, et al. Ito cells are liver-resident antigen-presenting cells for activating T cell responses. Immunity. 2007; 26:117–129. [PubMed: 17239632]

27. Zanchi AC, Gingold AR, Theise ND, Min AD. Necrotizing granulomatous hepatitis as an unusual manifestation of Lyme disease. Dig Dis Sci. 2007; 52:2629–2632. [PubMed: 17638077]

28. Zaidi SA, Singer C. Gastrointestinal and hepatic manifestations of tickborne diseases in the United States. Clin Infect Dis. 2002; 34:1206–1212. [PubMed: 11941547]

29. Warren A, et al. T lymphocytes interact with hepatocytes through fenestrations in murine liver sinusoidal endothelial cells. Hepatology. 2006; 44:1182–1190. [PubMed: 17058232]

30. Schmid GP. Epidemiology and clinical similarities of human spirochetal diseases. Rev Infect Dis. 1989; 11(Suppl 6):S1460–S1469. [PubMed: 2682958]

31. Norman MU, Hulliger S, Colarusso P, Kubes P. Multichannel fluorescence spinning disk microscopy reveals early endogenous CD4 T cell recruitment in contact sensitivity via complement. J Immunol. 2008; 180:510–521. [PubMed: 18097053]

32. Moriarty TJ, et al. Real-time high resolution 3D imaging of the Lyme disease spirochete adhering to and escaping from the vasculature of a living host. PLoS Pathog. 2008; 4:e1000090. [PubMed: 18566656]

33. Barbour AG. Isolation and cultivation of Lyme disease spirochetes. Yale J Biol Med. 1984; 57:521–525. [PubMed: 6393604]

34. Kawabata H, Norris SJ, Watanabe H. BBE02 disruption mutants of *Borrelia burgdorferi* B31 have a highly transformable, infectious phenotype. Infect Immun. 2004; 72:7147–7154. [PubMed: 15557639]

35. Ato M, et al. Loss of dendritic cell migration and impaired resistance to *Leishmania donovani* infection in mice deficient in CCL19 and CCL21. J Immunol. 2006; 176:5486–5493. [PubMed: 16622017]

36. Belperio JA, et al. Critical role for CXCR3 chemokine biology in the pathogenesis of bronchiolitis obliterans syndrome. J Immunol. 2002; 169:1037–1049. [PubMed: 12097412]

37. Faunce DE, Palmer JL, Paskowicz KK, Witte PL, Kovacs EJ. CD1d-restricted NKT cells contribute to the age-associated decline of T cell immunity. J Immunol. 2005; 175:3102–3109. [PubMed: 16116199]

38. Kajiwara T, et al. Effects of cyclosporin A on the activation of natural killer T cells induced by alpha-galactosylceramide. Transplantation. 2007; 27:184–192.

39. Benhnia MR, et al. Signaling through CD14 attenuates the inflammatory response to *Borrelia burgdorferi*, the agent of Lyme disease. J Immunol. 2005; 174:1539–1548. [PubMed: 15661914]
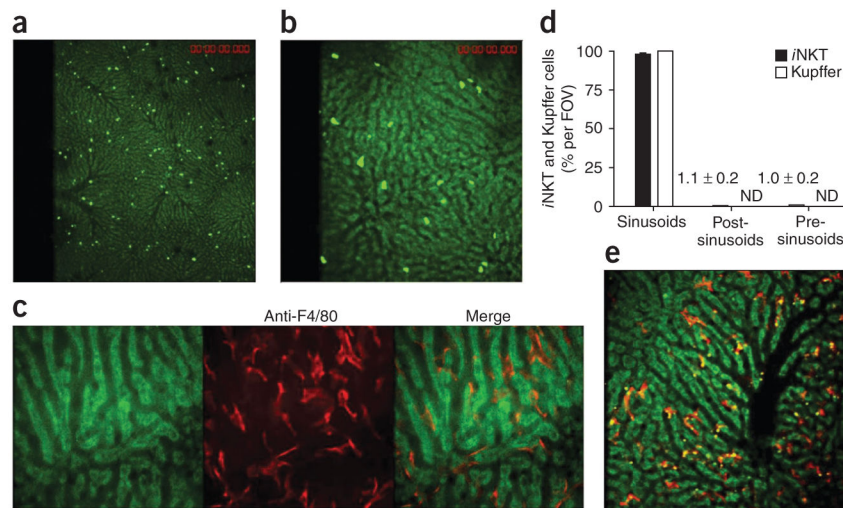
Figure 1.
Distribution of *i*NKT cells and Kupffer cells in the hepatic microvasculature. Spinning-disk confocal intravital microscopy of the vasculature of *Cxcr6*$^{gfp/+}$ and BALB/c mouse livers. (**a**,**b**) CXCR6$^+$ cells in the liver of *Cxcr6*$^{gfp/+}$ mice. (**c**) Liver-specific Kupffer cells (red) labeled with phycoerythrin-conjugated anti-F4/80 in the hepatic sinusoids of a BALB/c mouse. (**d**) GFP$^+$ cells and F4/80$^+$ cells in the sinusoids, post-sinusoidal venules and pre-sinusoidal venules of *Cxcr6*$^{gfp/+}$ mouse livers ($n = 7$ mice) in 21 FOV (*i*NKT cells) or 10 FOV (Kupffer cells). Numbers in graph indicate percent *i*NKT cells per FOV for bars not visible; ND, not detected. (**e**) Dextran conjugated to tetramethylrhodamine (2 megadalton; red) and polychromatic microspheres (green and yellow) bound to Kupffer cells. Original magnification, ×4 (**a** and *i*NKT cells in **d**), ×10 (**b**,**e** and Kupffer cells in **d**) or ×20 (**c**). Data are representative of more than three independent experiments (**a**–**c**,**e**) or seven experiments (**d**; error bars, s.e.m.).
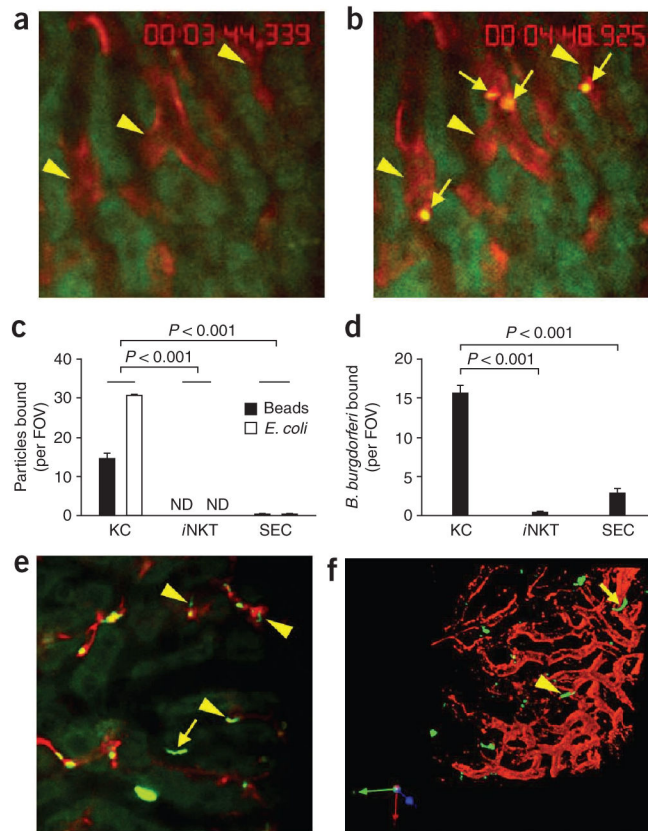
Figure 2.
Binding capacity of Kupffer cells, *i*NKT cells and SECs for beads and bacteria. (**a**,**b**) Microscopy of red Kupffer cells (arrowheads) before (**a**) and after (**b**) intravenous injection of polychromatic microspheres (arrows, **b**) into BALB/c mice. (**c**,**d**) Quantification of the binding of beads or *E. coli* (**c**) or *B. burgdorferi* (**d**) to Kupffer cells (KC), *i*NKT cells or SECs in *Cxcr6*gfp/+ mice given intravenous injection of polychromatic microspheres, or *E. coli* (**c**) or *B. burgdorferi* (**d**) expressing GFP or labeled with the red fluorescent nucleic acid stain Syto 60. (**e**) Binding of *B. burgdorferi* to the endothelium (arrow) as well as to Kupffer cells (arrowheads) in the hepatic sinusoids of a mouse treated as described in **d** (differences in activity, Supplementary Video 5). (**f**) Microcopy of *B. burgdorferi* in the liver of a mouse treated as described in **d**; yellow arrowhead indicates a GFP+ spirochete in the process of emigrating, and yellow arrow indicates a spirochete that has left the vasculature. Original magnification, ×20 (**a**,**b**,**e**,**f**). *P* values (**c**,**d**), Bonferroni's multiple-comparison test. Data are representative of more than three independent experiments (**a–e**) or two experiments (**f**).
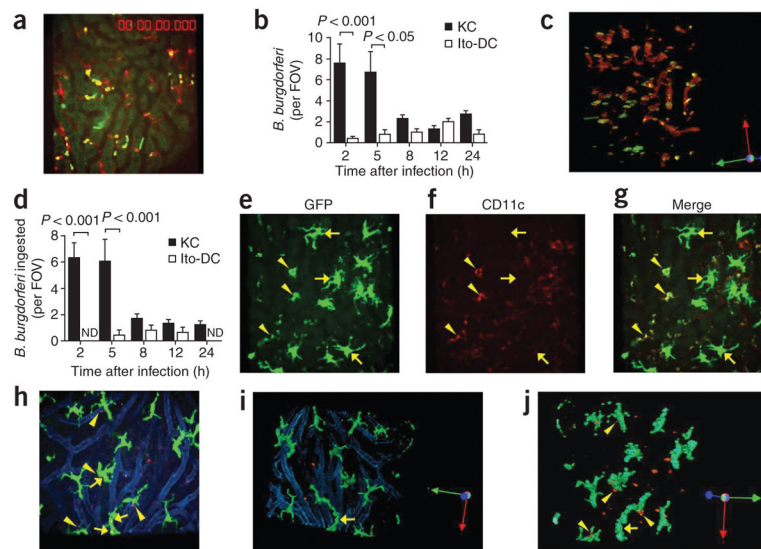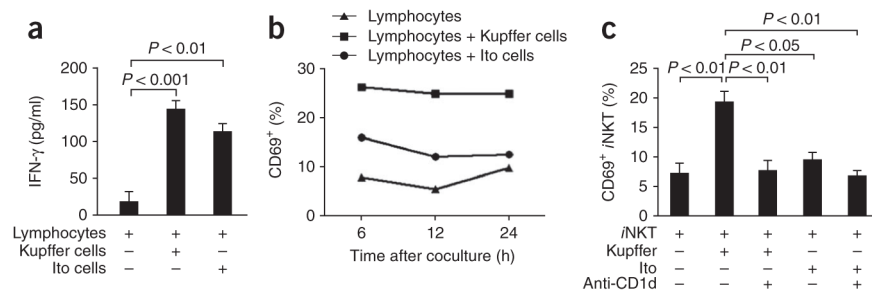
Figure 3.
Ingestion of *B. burgdorferi* by Kupffer cells and Ito cells. (**a**) Visualization of the hepatic vasculature of a *Cxcr6*$^{\text{gfp/+}}$ mouse at 2 h after the administration of GFP-expressing *B. burgdorferi* (yellow dots, shown interacting with red-labeled Kupffer cells). (**b**) Association of GFP-expressing or Tomato-expressing *B. burgdorferi* with Kupffer cells and Ito or dendritic cells (Ito-DC), measured in intravital videos of *Cxcr6*$^{\text{gfp/+}}$ and *Cx3cr1*$^{\text{gfp/+}}$ mice, respectively. (**c**) A *z*-stack reconstruction of two-dimensional microscopy, showing attachment and ingestion of spirochetes by Kupffer cells (rotation, Supplementary Fig. 1). (**d**) Total ingested *B. burgdorferi* confirmed after 360° rotation of *z*-stack-reconstructed images. (**e**–**g**) CD11c$^-$, GFP$^+$ big stellate (Ito) cells (arrows) and relatively small CD11c$^+$GFP$^+$ (dendritic) cells (arrowheads) in *Cx3cr1*$^{\text{gfp/+}}$ mouse liver. (**h**) Tomato-expressing *B. burgdorferi* bound by GFP$^+$ Ito cells in *Cx3cr1*$^{\text{gfp/+}}$ mouse liver. Arrows indicate associated spirochetes; arrowheads indicate spirochetes out of Ito cells. Vessels were stained with anti-PECAM-1 (blue). (**i,j**) Ingestion of Tomato-expressing *B. burgdorferi* by Ito cells, assessed after *z*-stack reconstruction. Original magnification, ×20 (**a,c,e**–**j**). *P* values (**b,d**), Bonferroni's multiple-comparison test. Data are representative of two independent experiments per group with more than four FOV each (**a–d,h–j**; error bars (**b,d**), s.e.m.) or two experiments (**e–g**).

Figure 4.
Antigen presentation by Kupffer cells and Ito cells. (**a**) Release of IFN-γ from liver-derived mixed-lymphocyte populations stimulated for 4 d with Kupffer or Ito cells isolated from BALB/c mice infected by injection of *B. burgdorferi*. (**b,c**) Expression of CD69 in mixed-lymphocyte populations treated as described in **a** (**b**) and a pure *i*NKT cell population isolated from *Cxcr6*$^{gfp/+}$ mice (Supplementary Methods) and cultured alone or together with Kupffer cells or Ito cells (as described in **a**) with or without anti-CD1d (**c**), evaluated by flow cytometry. *P* values (**a,c**), Bonferroni's multiple-comparison test. Data are representative of one experiment (mean and s.e.m. of three to four wells (**a**) or pooled cells from three to four wells (**b**)) or three independent experiments (**c**).
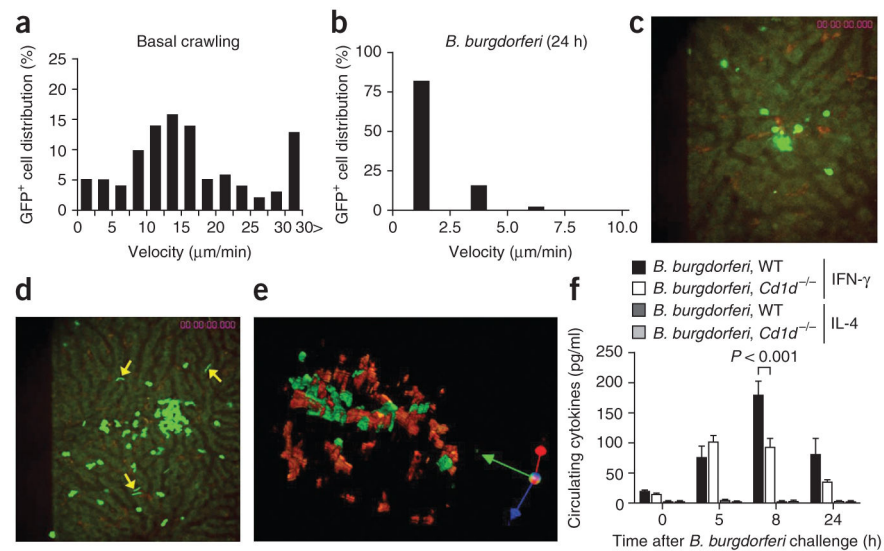
Figure 5.
Changes in *i*NKT cell activity after *B. burgdorferi* infection. (**a,b**) GFP$^+$ cell tracks in vehicle-treated mice (**a**) and at 24 h after injection of *B. burgdorferi* into *Cxcr6*$^{gfp/+}$ mice (**b**). (**c,d**) Distribution of GFP$^+$ *i*NKT cells and red-labeled Kupffer cells at 8 h (**c**) and 24 h (**d**) after injection of GFP-expressing *B. burgdorferi*. Arrows indicate surviving spirochetes. (**e**) A *z*-stack reconstruction showing Kupffer cells (red) and *i*NKT cells (green) at 24 h after infection. Original magnification, ×20 (**c,e**) or ×10 (**d**). (**f**) Enzyme-linked immunosorbent assay of IFN-γ and IL-4 in serum samples obtained from wild-type (WT) and *Cd1d*$^{-/-}$ mice before or 5, 8 or 24 h after *B. burgdorferi* injection. *P* values, Bonferroni's multiple-comparison test. Data are representative of three independent experiments with more than ten FOV (**a**) or more than two independent experiments (**b–e**) or one experiment with four to six mice per group (**f**; error bars, s.e.m.).
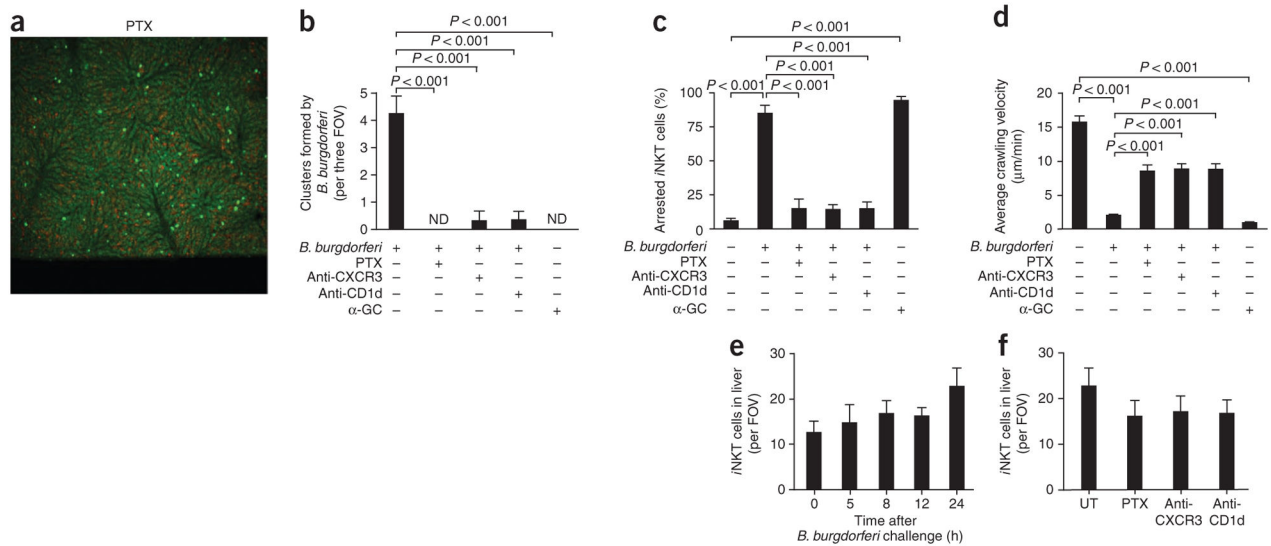
Figure 6.
Inhibition of *i*NKT cell cluster formation, average crawling velocity and stationary adhesion by pertussis toxin, anti-CXCR3 and anti-CD1d. Analysis of the hepatic microvasculature (visualized by spinning-disk confocal intravital microscopy) and formation of *i*NKT cell clusters (counted by intravital video) in *Cxcr6*$^{gfp/+}$ mice pretreated with pertussis toxin (PTX), anti-CXCR3, anti-CD1d and/or α-GalCer (α-GC) before injection of *B. burgdorferi*. (**a**) Distribution of *i*NKT cells after PTX treatment, assessed 24 h after infection. (**b**) Cluster formation by *B. burgdorferi* at 24 h after infection. Original magnification, ×4 (**a,b**). (**c,d**) Effect of pretreatment on the average crawling velocity (**c**) and stationary arrest (**d**) of *i*NKT cells at 24 h after infection. (**e**) Liver *i*NKT cells during the first 24 h of *B. burgdorferi* infection. (**f**) Effect of pretreatment on the number of *i*NKT cells in the liver sinusoids ($n =$ 4–6 mice per group). Original magnification, ×10 (**e,f**). *P* values (**b**–**d**), Bonferroni's multiple-comparison test. Data are representative of three experiments (**a**) or more than two independent experiments per group (**b**–**f**; error bars, s.e.m.).
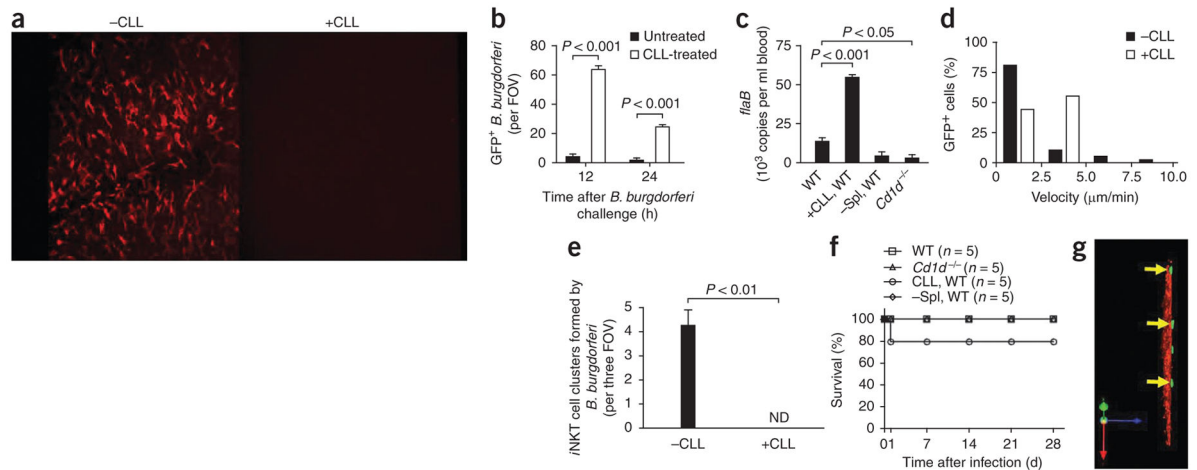
Figure 7.
Role of Kupffer cells in *B. burgdorferi* infection. (**a**) Kupffer cells labeled with anti-F4/80 before (-CLL) and 24 h after (+CLL) intravenous injection of CLLs (administered 24 h before *B. burgdorferi* infection to deplete mice of Kupffer cells). Original magnification, ×10. (**b**) Spirochetes remaining in the liver 12 h and 24 h after *B. burgdorferi* injection in untreated mice (-CLL) and CLL-treated mice (+CLL). (**c**) Spirochetes remaining in the blood 3 d after *B. burgdorferi* injection in untreated, CLL-treated and splenectomized (–Spl) wild-type mice and in *Cd1d*^{−/−} mice, assessed by quantitative PCR analysis of *B. burgdorferi* *flaB*. (**d**) Distribution of *i*NKT cell velocities at 5 h after spirochete challenge; nonfluorescent *B. burgdorferi* were administered to avoid possible confusion of GFP-expressing *B. burgdorferi* with GFP[+] *i*NKT cells in CLL-treated mice. (**e**,**f**) Formation of *i*NKT cell clusters at 24 h after *B. burgdorferi* infection. (**e**) Mortality of untreated, CLL-treated and splenectomized (-Spl) wild-type mice and of *Cd1d*^{−/−} mice after *B. burgdorferi* infection. (**g**) Migration of GFP-expressing spirochetes (arrows) out of microvasculature (space of Dissé) in a CLL-treated mouse. Original magnification, ×20. *P* values Bonferroni's multiple-comparison test (**b**) or Student's *t*-test (**c**,**e**). Data are representative of three experiments (**a**), more than two independent experiments per group (**b**,**d**,**e**,**g**), one experiment with duplicate pooled results of three mice (**c**) or one experiment with five mice per group (**f**; error bars (**b**,**c**,**e**), s.e.m.).

Table 1

B. burgdorferi clearance from mouse organs

	B. burgdorferi flaB (10^3 copies per mg tissue)				
	Bladder	**Heart**	**Joint**	**Liver**	**Spleen**
WT	16.8 ± 0.2	20.4 ± 1.7	2.3 ± 0.3	23.0 ± 9.4	10.5 ± 0.8
+CLL, WT	48.0 ± 0.2 ***	31.6 ± 1.5 **	12.9 ± 0.8 **	52.2 ± 5.7	25.9 ± 3.6 *
−Spl, WT	12.8 ± 1.2	17.8 ± 1.2	2.1 ± 0.4	36.8 ± 1.2	–
Cd1d$^{-/-}$	23.7 ± 1.5 *	10.4 ± 1.9 *	59.4 ± 0.6 ***	36.2 ± 1.1	10.9 ± 0.6

B. burgdorferi clearance in untreated, CLL-treated or splenectomized wild-type mice and in *Cd1d*$^{-/-}$ mice at 3 d after *B. burgdorferi* infection, assessed by quantitative PCR analysis of *B. burgdorferi flaB* (pooled DNA samples).

*
P < 0.05,

**
P < 0.01 and

***
P < 0.001, versus wild-type (Bonferroni's mutiple-comparison test).

Data represent one experiment with three to five mice, depending on experimental group (mean and s.e.m. of two independent measurements).